



RESEARCH ARTICLE

# A 100 W-level ultra-narrow fiber-coupled 780 nm diode laser

Longfei Jiang<sup>1,2,3,†</sup>, Rui Wang<sup>1,2,3,†</sup>, Huizi Zhao<sup>1,2,3</sup>, Jianyong Sun<sup>1,2,3</sup>, Qingshan Liu<sup>1,2,3</sup>,  
Zining Yang<sup>1,2,3</sup>, Hongyan Wang<sup>1,2,3</sup>, Weiqiang Yang<sup>1,2,3</sup>, Weihong Hua<sup>1,2,3</sup>, and Xiaojun Xu<sup>1,2,3</sup>

<sup>1</sup>College of Advanced Interdisciplinary Studies, National University of Defense Technology, Changsha, China

<sup>2</sup>Nanhu Laser Laboratory, National University of Defense Technology, Changsha, China

<sup>3</sup>Hunan Provincial Key Laboratory of High Energy Laser Technology, National University of Defense Technology, Changsha, China

(Received 6 May 2024; revised 26 June 2024; accepted 25 July 2024)

## Abstract

We report a high-power ultra-narrow fiber-coupled diode laser using a Faraday anomalous dispersion optical filter (FADOF) as an external cavity element. An external cavity suitable for both the fiber-coupled package and FADOF configuration has been proposed. Using a <sup>87</sup>Rb-based FADOF as the frequency-selective element, we realized a 103 W continuous laser output with a uniform circular beam. The center wavelength was precisely locked at the D<sub>2</sub> line of the Rb resonance, and the bandwidth was narrowed from 1.8 nm (free-running, full width at half maximum (FWHM)) to 0.013 nm (6.9 GHz, FWHM). The side mode suppression ratio reached 31 dB. Such diode lasers with precise wavelength and high spectral brightness have critical applications in many fields, such as high-energy gas laser pumping, spin-exchange optical pumping, Raman spectroscopy and nonlinear optics.

**Keywords:** diode lasers; external cavity; fiber coupling; optical filter; rubidium

## 1. Introduction

Electrically driven, compact, low-cost diode lasers are currently widely used. Commercial high-power diode lasers commonly have a 2–4 nm linewidth with a center wavelength drift of the order of 0.3 nm/A. However, many emerging applications require high-power diode lasers with fixed wavelengths and narrow spectra, such as spin-exchange optical pumping (SEOP)<sup>[1]</sup>, diode-pumped alkali lasers (DPALs)<sup>[2–5]</sup> and diode-pumped metastable rare gas lasers (DPRGLs)<sup>[6–9]</sup>. For this purpose, methods have to be applied to realize wavelength locking and linewidth narrowing of high-power diode lasers.

The most commonly used method is constructing an external cavity, which employs wavelength selective elements to modulate the mode competition. These lasers are known as external cavity diode lasers (ECDLs). For high-power

diode lasers, the external cavities are constructed mainly by plane gratings or volume Bragg gratings (VBGs). Based on plane gratings, Zhdanov *et al.*<sup>[10]</sup> achieved 10 W output with an 11 GHz linewidth centered at 852 nm. Yang *et al.*<sup>[11]</sup> obtained a spectral bandwidth of less than 15 GHz with a central wavelength of 780 nm and 10 W output. Hersman *et al.*<sup>[12]</sup> proposed a kilowatt-level design and tested a prototype system. To conclude, the plane grating-based external cavity has the merits of a wide tunable range and narrow linewidth. However, it has a relatively low efficiency and damage threshold, which limits its application in high-power diode lasers. Based on VBGs, Yang *et al.*<sup>[13]</sup> realized wavelength locking on a 780 nm single bar, achieving 80 W power with 0.1 nm linewidth and 90% power extraction efficiency. Koenning *et al.*<sup>[14,15]</sup> investigated linewidth-narrowed diode lasers for DPAL pumping, firstly achieving 1 kW output of a 780 nm diode stack with a spectral width of less than 0.1 nm, and then realized a fiber-coupled 766 nm diode laser exceeding 3 kW with 30 GHz bandwidth. Han *et al.*<sup>[16]</sup> utilized a different structure of a VBG-based external cavity and realized a 780 nm diode laser with a spectral width of 0.138 nm and output power of 1090 W. The VBG-based external method is beneficial for

Correspondence to: Z. Yang and H. Wang, College of Advanced Interdisciplinary Studies, National University of Defense Technology, Changsha 410073, China. Emails: yangzining09@nudt.edu.cn (Z. Yang); wanghongyan@nudt.edu.cn (H. Wang)

<sup>†</sup>These authors contributed equally to this work.

high efficiency and compactness, but a complex temperature control system is needed due to the wavelength drift of the VBG (8–10 pm/K)<sup>[17–19]</sup>.

A new method using a Faraday anomalous dispersion optical filter (FADOF) in the external cavity shows potential for precise wavelength locking of high-power diode lasers. The FADOF is a kind of optical filter that allows precise wavelength-related transmittance of atomic (usually alkali atoms) absorption lines. The FADOF's optical filtering function originates from the hyperfine sublevels of the alkali elements, and makes the transmission spectra exhibit a complicated multi-peak form. As a filter, the FADOF has the properties of extremely narrow spectral linewidth and high noise rejection ability. Chen's group reported an FADOF, the gain factor of which can be larger than 25,000 (44 dB) within a bandwidth as narrow as 13 MHz in 2018<sup>[20]</sup> and further achieved an ultra-narrow bandwidth of 6.6 MHz by using cold atoms to reduce the linewidth<sup>[21]</sup>. The FADOF can also act as an external cavity element because of its role in frequency selection. ECDLs using FADOFs as the frequency-selective elements have been named 'Faraday lasers'<sup>[22,23]</sup>. In 2019, Chang *et al.*<sup>[24]</sup> demonstrated the first Cs Faraday laser, which offered a stable output frequency exactly set by the peak transmission frequency of the Cs D<sub>2</sub> line. In 2020, Shi *et al.*<sup>[25]</sup> demonstrated a dual-frequency Faraday laser operating on a Cs D<sub>2</sub> line. The laser linewidth of each laser mode is narrower than 33 kHz, and the frequency difference between the two modes is tunable over a range of 1.4 GHz.

Recently, high-power diode lasers using an FADOF-based external cavity have made some development due to the emerging requirement for high-energy gas laser pumping, SEOP, quantum optics, etc. In 2018, Rotondaro *et al.*<sup>[26]</sup> achieved an 852 nm diode laser with a power output of 518 W based on a Cs FADOF, with a spectral linewidth narrowed from the broadband 3 THz to 10 GHz and retaining 80% of the original power. In 2021, Tang *et al.*<sup>[27]</sup> proposed a configuration with an adjustable feedback ratio. A <sup>85</sup>Rb FADOF-based external cavity was used to precisely lock the center wavelength to the Rb resonance D<sub>2</sub> line. The bandwidth was narrowed from 4 nm in free-running to 0.002 nm (1.2 GHz, full width at half maximum (FWHM)), achieving an average power of 18 W. In 2022, Tang *et al.*<sup>[28]</sup> further improved the optical path structure to build an FADOF that was insensitive to the polarization of the input light, expanding the FADOF-based method to the case of non-polarized diode lasers, achieving a 38.3 W output with a 0.005 nm (2.6 GHz, FWHM) linewidth.

Currently, diode lasers are commonly packaged with fiber coupling, which is beneficial for uniform round beam shape generation and flexible applications. Up to now, the FADOF-based external cavity has not been applied for fiber-coupled diode lasers. In this paper, the wavelength locking and linewidth narrowing of a 780 nm fiber-coupled diode module using a Rb FADOF have been conducted, achieving a

CW output power over 100 W and ultra-narrow linewidth on the level of 0.01 nm.

## 2. Experiment setup and results

### 2.1. Study of FADOF characteristics

Firstly, we used a probe laser to measure the transmission spectra of the FADOF, which will be used as the feedback element in the external cavity. The alkali vapor cell was filled with pure <sup>87</sup>Rb without buffer gas. The diameter of the cell was 25.4 mm, and the length was 60 mm. The windows were coated with anti-reflection coating on the exterior surfaces. Aluminum was sleeved outside the cell and was heated by a resistance wire. A thermocouple was embedded in the heating sleeve to monitor the cell temperature. The temperature control system, including the aluminum, resistance wire, thermocouple and control circuits, could realize temperature control with 1°C precision. Figure 1 shows the schematic of the Rb cell, the magnets and the heating system.

The magnetic field was excited by a pair of permanent magnets and was parallel to the direction of light transmission. The strength of the magnetic field at the center of the cell was about 110 G, measured by a digital magnetometer with an accuracy of 0.1 G.

Figure 2 shows the experimental setup of the FADOF transmission spectrum measurement. A 780 nm single-frequency distributed Bragg reflection (DBR) probe laser (DBR801-780, UniQuanta) was used to measure the spectral characteristics of the FADOF. The bandwidth of the probe laser was less than or equal to 1 MHz and the tuning range was  $\pm 2$  nm. The probe light first passed through a polarization beam splitter (PBS), PBS<sub>1</sub>, to produce linearly polarized light. The light reflected by PBS<sub>1</sub> was used to monitor the wavelength in real time. The light transmitted by PBS<sub>1</sub> was then split into two beams by a beam splitter (BS). One was set as a reference light and was detected by a photodetector (PD), PD<sub>1</sub>. The other beam entered the cell and interacted with the atoms. The polarization state of the light changed as it passed through the cell, and the rotation

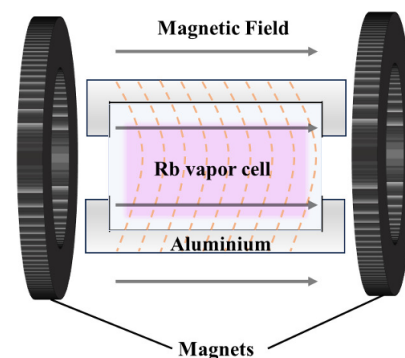
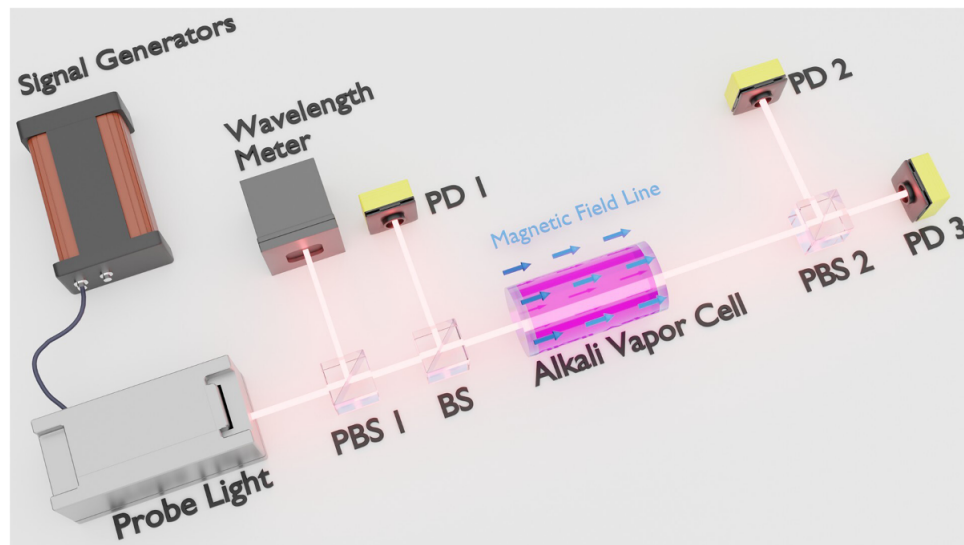


Figure 1. Schematic of the Rb cell, the magnets and the heating system.



**Figure 2.** Schematic of the experimental setup of the FADOF's transmission spectrum measurement. BS, beam splitter; PBS, polarization beam splitter; PD, photodetector.

angle was closely related to the wavelength of light. Only when the rotation angle was  $90^\circ$  could the light be reflected entirely by  $\text{PBS}_2$ , which was equally placed as  $\text{PBS}_1$ . In this condition, the signal detected by  $\text{PD}_2$  reached the maximum. The other part of the light was detected by  $\text{PD}_3$ . At the same time, alkali metal atoms also absorbed light with a wavelength near the atomic absorption line. A combination of different factors contributed to the transmission spectrum of the FADOF. The transmission characteristics of the FADOF determined the operation state of the entire external cavity laser. The experiment was carried out under a series of cell temperatures, including  $90^\circ\text{C}$ ,  $100^\circ\text{C}$ ,  $110^\circ\text{C}$  and  $120^\circ\text{C}$ . Figure 3 shows the transmission spectra the experiment obtained. The blue line in Figure 3 represents the transmission property of the FADOF, which was defined to represent the proportion of the incident light whose polarization direction altered by  $90^\circ$  exactly after passing through the Rb cell. A higher value in the blue line represents a better filtering effect of the FADOF, which is more favorable when using it as a frequency-selective element in the diode laser external cavity. Experimentally, it was calculated by the ratio of the light intensity detected at  $\text{PD}_2$  and the total input intensity ( $\text{PD}_1 + \text{PD}_2 + \text{PD}_3$ ). The pink line in Figure 3 represents the transmission property of the cell, which was defined to represent the proportion of the incident light's weakening after passing through the cell, which reflects the absorption effect of the alkali atoms. Experimentally, it was calculated by the sum of light intensity detected at  $\text{PD}_2$  and  $\text{PD}_3$ , dividing the total input intensity ( $\text{PD}_1 + \text{PD}_2 + \text{PD}_3$ ).

The length of the cell and the magnetic strength were constant during the experiment, while we changed the atomic concentration to modulate the operation state of the system. We changed the temperature to alter the saturated vapor

pressure; thus, the atomic concentration was regulated. In the experiment, the measured peak transmittance was 86.8%. It should be noted that losses due to the cell windows were taken into account during the experiments, and were mainly caused by the uncoated inner surfaces of the cell. Considering these factors, it can be deduced that the transmittance of the medium can be up to around 95%.

## 2.2. External cavity diode laser construction and experimental results

We proposed an external cavity diode laser module with an adjustable optical feedback ratio based on a fiber-coupled diode laser, and the configuration can be seen in Figure 4.

The diode laser module we used was from Suzhou Everbright Photonics, and had 18 emitters and 144 W output power at the maximum drive current of 11 A. The emitters in each column were combined by reflectors, as shown in Figure 5. The facet of the emitters was coated with anti-reflective film with a residual reflectivity of less than 0.5% to improve the efficiency of external cavity feedback. After being combined and focused, the light beams from the 18 diode emitters were coupled into the optical fiber with a  $135\ \mu\text{m}$  core diameter. The output laser was collimated by a collimator with  $f = 50\ \text{mm}$  and then divided into two orthogonal linearly polarized beams at  $\text{PBS}_1$ . Rotating the half-wave plate changed the polarization angle of the linearly polarized light, altering the ratio of transmitted light to reflected light at  $\text{PBS}_2$ . The optical path is divided into two main parts: the feedback optical path and the output optical path. The light beam transmitted by  $\text{PBS}_2$  was led into the feedback optical path. The light beam reflected by  $\text{PBS}_2$  was then reflected by 'Reflector 1' and then combined

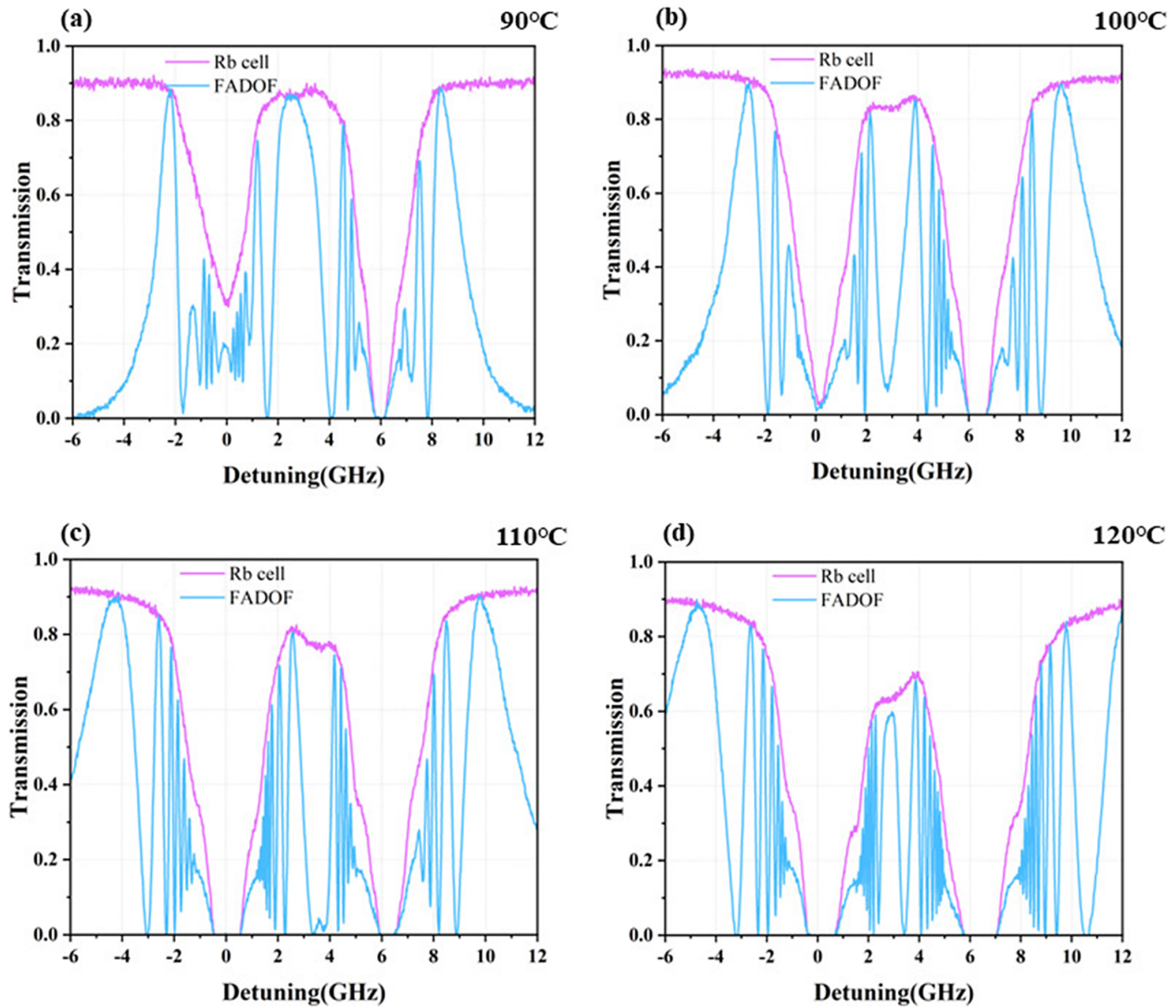


**Figure 3.** Transmission spectra of the Rb cell and the FADOF. Subfigures (a)–(d) represent the results for cell temperatures of 90°C, 100°C, 110°C and 120°C.

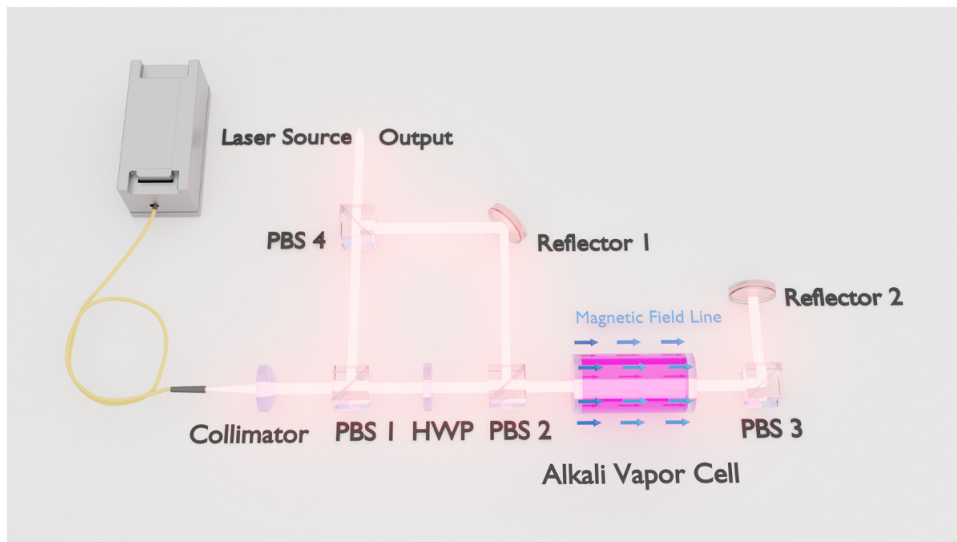


**Figure 4.** Schematic of the experimental setup of an FADOF-based external cavity diode laser. PBS, polarization beam splitter; HWP, half-wave plate.

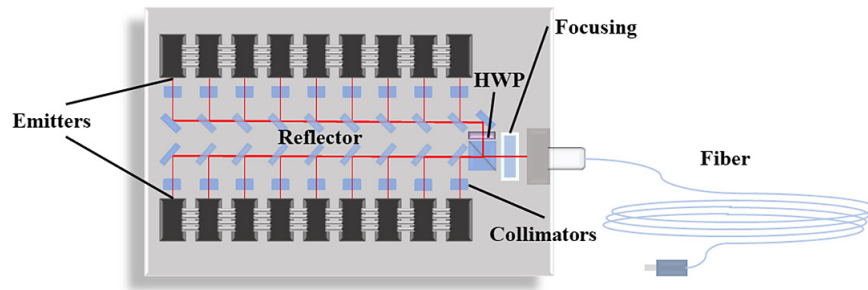


Figure 5. Schematic of the internal structure of the fiber-coupled diode laser. HWP, half-wave plate.

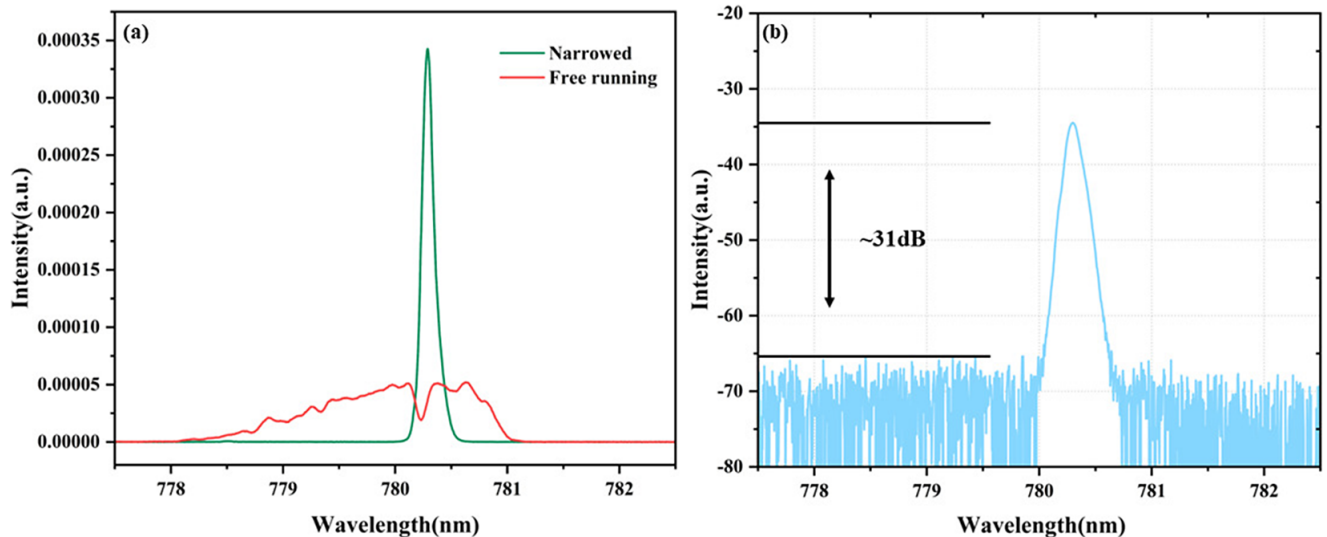


Figure 6. (a) Measured spectra of the free-running and the locked diode laser. (b) Spectrum of the ECDL in log scale.

at  $PBS_4$  with the reflected beam from  $PBS_1$  to form the final output beam. A half-wave plate and  $PBS_2$  combination was used in the feedback branch to modulate the feedback ratio. Rotating the half-wave plate changed the polarization angle of the linearly polarized light, ultimately changing the power of the transmitted light at  $PBS_2$ . The transmitted light entered the cell and interacted with the atoms. The polarization state of light changed as it passed through the cell, and the rotation angle was closely related to the wavelength of light. As the rotation angle approached  $90^\circ$ , more light would be reflected by  $PBS_3$ . This part of the light was reflected by a high reflector and went back into the fiber core and, finally, the diode laser emitters, forming an external cavity. The mode competition within the diode laser was changed after feedback, and the mode corresponding to the feedback light gained a competitive advantage over the free-running mode. When the feedback ratio was strong enough, the diode laser tended to lase in the external cavity mode, resulting in a precisely locked wavelength and ultra-narrow linewidth.

The spectra of the diode laser were measured as follows: a small portion of the output light was fed into an integrated sphere, and the entire spectra of all the emitters were measured by an optical spectrum analyzer (OSA, Yokogawa

AQ6370D) with a resolution of 0.02 nm. The spectra were analyzed at different cell temperatures from  $90^\circ\text{C}$  to  $130^\circ\text{C}$ . Several criteria were followed when selecting the optimal heating temperature. Firstly, realize the stable operation of the entire laser system without mode hopping. Secondly, minimize linewidth and increase the side mode suppression ratio (SMSR). Following the above principles, the optimized cell temperature was  $110^\circ\text{C}$ . At this condition, the central wavelength was 780.24 nm with an SMSR of 31 dB, as shown in Figure 6.

In the experiment, we noticed the power loss caused by constructing an external cavity, and relevant measurements were conducted. We measured the laser power before and after constructing the external cavity under conditions ranging from 2 to 11 A, and the results are shown in Figure 8. The output power reaches 103 W at 11 A, as tested by an Ophir power meter, and the external cavity efficiency is 71%. Considering the losses caused by the optical elements, the actual ratio of the FADOF feedback is approximately 20%.

Due to the limited resolving ability of the OSA, we further used a scanning Fabry–Pérot interferometer to realize high-resolution spectrum measurements; see Figure 7. The free spectral range of the interferometer was 10 GHz with

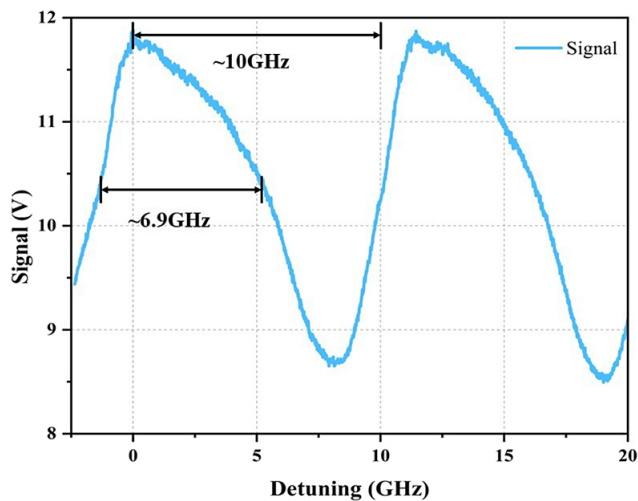


Figure 7. The Fabry–Pérot spectrum of the FADOF-based ECDL.

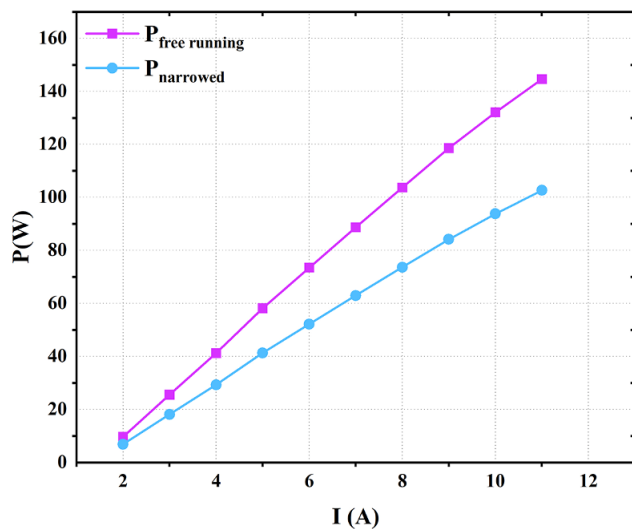


Figure 8. The output power of the free-running (purple) and the locked (blue) diode laser with respect to the drive current.

a resolution of 67 MHz in the free-running case. In the experiment, the spectrum of the laser module was 6.9 GHz at a maximal power of 103 W and heating temperature of 110°C.

### 3. Discussion

To begin with, the efficiency of the FADOF-based external cavity is discussed. In the experiment, we observed that the fiber-coupled configuration required more feedback (~30%) to achieve the same SMSR as the free-space configuration (~20%)<sup>[27]</sup>, which mainly resulted from the different coupling efficiency between the diode emitter and the feedback light. For the fiber-coupled configuration, the feedback intensity was weakened due to the change in beam shape when the feedback light was transmitted through the fiber.

In addition, we consider that the uncoated window's inner surfaces also weaken the feedback. To improve the feedback effect, we will further optimize the coupling conditions, including the feedback configuration, the fiber core diameter, and the emitter's facet reflectivity.

Secondly, the spectral stability is analyzed. The experiment achieved reasonable results as mentioned above. At the same time, we noticed that tiny wavelength changes (~0.01 nm) occurred when the water temperature changed to an extent of approximately 5°C. The following explanations are made concerning this phenomenon. When the water temperature changed, the gain curve of the diode laser drifted. As the transmission spectrum of the FADOF had peaks with similar transmittance, the mode competition inside the diode laser could be changed, resulting in an unstable output central wavelength. In addition, sideband counterparts became dominant modes of mode competition. To increase the system stability, we will further make some improvements to the FADOF, such as flushing in buffer gas to suppress the sideband<sup>[29]</sup>. When the sideband is suppressed, the bandwidth can be reduced, and the FADOF will have only a single transmittance peak. Due to the above factors, there is still much room for optimization of the current technical route.

Thirdly, we discuss the thermal effect of the FADOF. In this experiment, no significant temperature rise in the cell was observed, indicating that the whole cell thermal effect was small. The absorption of the alkali vapor was remarkably weak for a number of reasons. Firstly, without buffer gas, the Rb vapor has a very narrow absorption linewidth (~0.6 GHz). While the intra-cavity circulating diode laser has a relatively broad bandwidth (~6.9 GHz), the Rb vapor absorbs only a small amount of energy. Secondly, based on the measured transmission spectra of the FADOF, the transmission peaks are separated from the absorption line, which also weakens the absorption effect and ultimately reduces the thermal effect. In this circumstance, the FADOF can reach a high upper limit of the loaded power capacity as an external cavity element for high-power diode lasers.

Compared with the traditional wavelength-locking method, FADOF-based high-power diode lasers have some unique characteristics. One is the high wavelength accuracy; the center wavelength of the FADOF-based laser is strictly locked to the atomic filter's line, and is totally unaffected by the fluctuation of the cooling temperature and the drive current. As with pumping sources, for example, for alkali or metastable inert atoms, the light–atom interaction could be the strongest due to the precise wavelength match. Secondly, the linewidth is at least an order of magnitude narrower than that of the VBG method, which could decrease the buffer gas pressure requirements in the usual alkali-based systems. Such high-power diode lasers with high spectral brightness will have wide applications in high-energy gas lasers, SEOP, Raman spectroscopy, frequency conversion, etc.

#### 4. Conclusion

In conclusion, we used an FADOF-based external cavity to realize precise wavelength locking and linewidth narrowing of a fiber-coupled diode laser. A special external cavity, which is suitable for both the fiber-coupled package and the polarization requirement of the FADOF, has been proposed and verified. A power of over 100 W has been realized, with a wavelength strictly locked to the Rb D<sub>2</sub> line and linewidth of the order of 0.01 nm. Based on the experimental results, some current limitations are analyzed, and further scaling routes are proposed. The power improvement of such ultra-narrow high-power diode lasers will extend their applications to a wide range of fields.

#### Acknowledgements

The authors thank Prof. Jingbiao Chen and his group (Institute of Quantum Electronics, Department of Electronics, Peking University) for their theoretical support in terms of the FADOF calculation. The authors also thank Dr. Hao Yu (Suzhou Everbright Photonics Co., Ltd.) for his technical support in the diode laser operations.

#### References

1. N. Whiting, P. Nikolaou, N. A. Eschmann, M. J. Barlow, R. Lammert, J. Ungar, W. Hu, L. Vaissie, and B. M. Goodson, *Appl. Phys. B* **106**, 775 (2012).
2. W. F. Krupke, R. J. Beach, V. K. Kanz, and S. A. Payne, *Opt. Lett.* **28**, 2336 (2003).
3. B. V. Zhdanov, M. D. Rotondaro, M. K. Shaffer, and R. J. Knize, *Opt. Commun.* **354**, 256 (2015).
4. A. V. Bogachev, S. G. Garanin, A. M. Dudov, V. A. Yeroshenko, S. M. Kulikov, G. T. Mikaelian, V. A. Panarin, V. O. Pautov, A. V. Rus, and S. A. Sukharev, *Quantum Electron.* **42**, 95 (2012).
5. G. A. Pitz, D. M. Stalnaker, E. M. Guild, B. Q. Oliner, P. J. Morana, S. W. Townsend, and D. A. Hostutler, *Proc. SPIE* **9729**, 972902 (2016).
6. J. Han and M. C. Heaven, *Opt. Lett.* **37**, 2157 (2012).
7. Z. Yang, G. Yu, H. Wang, Q. Lu, and X. Xu, *Opt. Express* **23**, 13823 (2015).
8. J. Han, M. C. Heaven, P. J. Moran, G. A. Pitz, E. M. Guild, C. R. Sanderson, and B. Hokr, *Opt. Lett.* **42**, 4627 (2017).
9. R. Wang, Z. Yang, Q. Liu, K. Han, H. Wang, and X. Xu, *Opt. Lett.* **47**, 3279 (2022).
10. B. V. Zhdanov, T. Ehrenreich, and R. J. Knize, *Electron. Lett.* **43**, 221 (2007).
11. Z. Yang, Y. Li, H. Wang, Q. Lu, and X. Xu, *Chin. Opt. Lett.* **9**, 60 (2011).
12. F. W. Hersman, J. H. Distelbrink, J. Ketel, J. Wilson, and D. W. Watt, *Proc. SPIE* **9729**, 972905 (2016).
13. Z. Yang, H. Wang, Q. Lu, W. Hong, and X. Xu, *Chin. Phys. Lett.* **28**, 104202 (2011).
14. T. Koenning, D. Irwin, D. Stapleton, R. Pandey, S. Patterson, and T. Guiney, *Proc. SPIE* **8962**, 89620F (2014).
15. T. Koenning, D. McCormick, D. Irvin, D. Stapleton, T. Guiney, and S. Patterson, *Proc. SPIE* **9348**, 934805 (2015).
16. J. Han, J. Zhang, X. Shan, Y. Zhang, H. Peng, L. Qin, and L. Wang, *Optik* **264**, 169455 (2022).
17. B. Liu, H. Liu, P. Zhu, and X. Liu, *Opt. Commun.* **486**, 126792 (2021).
18. J. Han, J. Zhang, X. Shan, H. Peng, Y. Zhang, L. Qin, and L. Wang, *Opt. Laser Technol.* **159**, 108974 (2023).
19. D. Xu, D. Ma, Z. Yu, L. Xu, and X. Chen, *Proc. SPIE* **11262**, 112620C (2020).
20. D. Pan, T. Shi, B. Luo, J. Chen, and H. Guo, *Sci. Rep.* **8**, 6567 (2018).
21. X. Guan, W. Zhuang, T. Shi, J. Miao, J. Zhang, J. Chen, and B. Luo, *Front. Phys.* **10**, 1090483 (2022).
22. T. Endo, T. Yabuzaki, M. Kitano, T. Sato, and T. Ogawa, *IEEE J. Quantum Electron.* **13**, 866 (1977).
23. Z. Xu, X. Xue, D. Pan, X. Zhang, W. Zhuang, and J. Chen, *Chin. Sci. Bull.* **59**, 3543 (2014).
24. P. Chang, Y. Chen, H. Shang, X. Guan, H. Guo, J. Chen, and B. Luo, *Appl. Phys. B* **125**, 230 (2019).
25. T. Shi, X. Guan, P. Chang, J. Miao, D. Pan, B. Luo, H. Guo, and J. Chen, *IEEE Photonics J.* **12**, 1503211 (2020).
26. M. D. Rotondaro, B. V. Zhdanov, M. K. Shaffer, and R. J. Knize, *Opt. Express* **26**, 9792 (2018).
27. H. Tang, H. Zhao, R. Wang, L. Li, Z. Yang, H. Wang, W. Yang, K. Han, and X. Xu, *Opt. Express* **29**, 38728 (2021).
28. H. Tang, H. Zhao, D. Zhang, L. Li, W. Yang, K. Han, Z. Yang, H. Wang, and X. Xu, *Opt. Express* **30**, 29772 (2022).
29. J. Xiong, B. Luo, L. Yin, J. Chen, and H. Guo, *IEEE Photon. Technol. Lett.* **30**, 716 (2018).